Journal of Building Engineering 102 (2025) 111996

Contents lists available at ScienceDirect

Journal of Building Engineering

journal homepage: www.elsevier.com/locate/jobe

The effect of calcined clay reactivity on the mechanical properties and chloride diffusion resistance of alkali-activated calcined clay-GGBFS concrete

Samuel De Carvalho Gomes [a], Yu Pang [a,*], Quang Dieu Nguyen [a,**], Wengui Li [a,b], Kirk Vessalas [a], Arnaud Castel [a]

[a] School of Civil and Environmental Engineering, University of Technology Sydney (UTS), Sydney, NSW 2007, Australia
[b] Centre for Infrastructure Engineering and Safety, School of Civil and Environmental Engineering, The University of New South Wales, NSW, 2052, Australia

ARTICLE INFO

Keywords:
Calcined clay
GGBFS
Alkali-activated concrete
Bulk diffusion
Modified-RCPT
Resistivity
Rapid Migration test
NT BUILD 492
Pore Structure
pH values
XRD
calcined clay reactivity

ABSTRACT

The increasing demand for sustainable and durable construction materials, particularly in aggressive environments such as those exposed to chloride ingress, necessitates the exploration of alternative binders that offer enhanced performance and lower environmental impact compared to traditional Portland cement. This study investigates the chloride resistance of calcined clay/ground granulated blast furnace slag (GGBFS) geopolymer concretes, focusing on variations in precursor proportions, alkali activator concentrations, and the amorphous content of two calcined clays. Durability tests, including standard bulk chloride diffusion, modified-rapid chloride permeability test (RCPT-10V), and NT Build 492, were conducted to evaluate the concrete performance. The compressive strength achieved ranged from 31.5 to 63.5 MPa. Notably, high-grade calcined clay with a 10 % Na_2O achieved the highest compressive strength of 63.5 MPa. Electrical resistivity tests indicated that free ions in the pore solution, especially unbound alkalis, contributed to increase the conductivity. A correlation between RCPT results and chloride diffusion coefficients categorized most concretes as low performers in chloride environments, with the exception of the 50HG50S-10 sample, which was categorized as medium performance. Notably, increasing the Na_2O concentration improved the chloride resistance of low-grade calcined clay, and this was further enhanced with high-grade calcined clay. Finally, exposure to NaCl resulted in no new phases except for halite in low-grade calcined clay. No Friedel's salt was detected in any sample.

1. Introduction

Alkali-activated materials (AAMs), commonly referred to as geopolymers, are produced by combining aluminosilicate-containing precursors such as fly ash and ground granulated blast furnace slag (GGBFS) with alkalis to form alkali-activated binders. While fly ash and GGBFS are industrial by-products with varying compositions, they are highly suitable for the alkali activation process. AAMs offer

* Corresponding author.
** Corresponding author.
E-mail addresses: yu.pang@student.uts.edu.au (Y. Pang), quangdieu.nguyen@uts.edu.au (Q.D. Nguyen).

https://doi.org/10.1016/j.jobe.2025.111996
Received 14 November 2024; Received in revised form 23 January 2025; Accepted 31 January 2025
Available online 1 February 2025

a low embodied carbon alternative to Portland cement-based concrete, aligning with the construction industry's increasing focus on sustainability. The durability of these materials has been extensively studied, as it is a critical factor influencing their acceptance within the industry, which adheres to specific standards [1]. Over recent years, extensive research has focused on alkali-activated concrete (AAC) due to its environmentally friendly nature and notable performance advantages. These benefits include enhanced resistance to acids and sulfates, improved heat resistance, and higher early strength [2].

The complete understanding of the long-term durability of alkali-activated materials is still under investigation, with further research needed to uncover potential mechanisms and improvements. An important area that requires attention is the study of how AAMs are able to resist corrosion of steel reinforcement over time [3,4]. Following the 1950s, the focus shifted from carbonation to chloride attack as the primary cause of steel corrosion in reinforced concrete structures [5]. The marine environment poses significant challenges to the durability of reinforced concrete, particularly in terms of corrosion. The presence of chloride and sulfate salts in seawater can penetrate the concrete through its interconnected pores, leading to concrete degradation, steel corrosion, and reduced load-carrying capacity. Moreover, maintenance costs are substantial, with global expenditure on preventing, mitigating, and repairing damage to civil infrastructure amounting to approximately US $2.2–2.5 trillion per year or over 3.0–3.4 % of the world's GDP [2,6]. Hence, it is crucial to utilize high-grade concrete materials that have low permeability to chloride in order to construct resilient reinforced concrete structures.

Alkali-activated GGBFS, commonly known as alkali-activated slag (AAS), is an emerging material in the field of sustainable construction materials, gaining traction for its lower carbon footprint compared to traditional Portland cement [7]. One of the significant advantages of alkali-activated slag is its improved resistance to chloride ion penetration, a critical factor in extending the lifespan of structures exposed to aggressive marine environments or deicing salts [8]. Several studies have examined the chloride resistance of alkali-activated slag and found that it generally exhibits a lower chloride diffusion coefficient and a higher chloride binding capacity compared to ordinary Portland cement [9]. Moreover, studies have shown that the resistance to chloride diffusion resistance in alkali-activated slag systems can vary depending on their formulation. However, when properly optimized with suitable activators, these systems demonstrate exceptional resistance to chloride penetration, making them a viable option for maritime and industrial applications where protection against chloride is crucial [10].

The widespread application of alkali-activated GGBFS presents certain challenges. Concerns have been raised about GGBFS availability as a limited resource, which may hinder its ability to replace a significant portion of global cementitious binders [11]. Additionally, AAS faces issues such as poor workability, rapid setting, and excessive shrinkage. To address these drawbacks, researchers have recently turned their attention to binary systems that utilize low calcium precursors like fly-ash, metakaolin or calcined clays [6]. In alkali-activated materials, two primary systems emerge based on their calcium content. Low-calcium systems, such as alkali-activated Class F fly-ash (AAFA) and alkali-activated metakaolin (AAMK), predominantly produces sodium aluminosilicate hydrate (N-A-S-H) gels as the main reaction products. Conversely, high-calcium systems, exemplified by alkali-activated GGBFS (AAS), primarily forms calcium aluminosilicate hydrate (C-A-S-H) gels with a structure similar to tobermorite. In mixed alkali-activated systems, both N-A-S-H and C-A-S-H gels may coexist [12]. The development of different phases in alkali-activated materials significantly influences their pore structure and chloride-binding capabilities. While N-A-S-H gels exhibit a more porous microstructure, they also have higher chloride-binding capacity due to their larger surface area. However, this same porous nature negatively impacts their overall chloride diffusion resistance, making C-A-S-H gels more effective in this regard [6,13,14].

Research conducted by Rakhimova et al. demonstrated promising advancements in the utilization of calcined clay and GGBFS in geopolymer concretes to enhance their mechanical properties [15]. The combination of slag and calcined clay was chosen due to their complementary properties, which can improve both mechanical strength and durability of concrete. In alkali-activated systems, slag primarily forms C-A-S-H gels, while calcined clay promotes N-A-S-H gel formation, creating a denser microstructure that can enhance both compressive strength and chloride diffusion resistance [16]. The combination of GGBFS with calcined clay (containing 60 % amorphous phase composed of kaolinite/montmorillonite) proved to be effective as a secondary precursor in blended alkali-activated systems. Optimal results were achieved when using a composition ratio a 70/30 composition ratio for alkali-activated GGBFS/calcined clay, activated with a 4 M NaOH solution. As a result, the compressive strength reached up to 30 MPa after a curing period of 28 days. Gomes et al. conducted a study on the physical and mechanical performance of alkali-activated materials, as well as their resistance to accelerated carbonation, using low-grade calcined clay combined with GGBFS [17,18]. The objective was to evaluate the impact of increasing GGBFS content on mortar properties, specifically the presence of Ca-rich phases like C-(A)-S-H/C-(N)-A-S-H, which contributed to improved microstructure densification. Additionally, higher GGBFS content resulted in increased pH levels, enhancing resistance against carbonation. However, neither of these studies investigated concrete durability in chloride-rich environments. Thus, further research is needed to examine the chloride diffusion resistance of alkali-activated calcined clay-GGBFS concrete in detail.

This study investigates the chloride diffusion resistance of binary calcined clay and ground granulated blast furnace slag (GGBFS) alkali-activated concretes. The research examines how varying precursor proportions, alkali activator concentrations, and amorphous content in low-grade and high-grade calcined clays affect the durability and mechanical properties of the concrete. Durability tests, including water absorption, volume of permeable voids (VPV), resistivity, bulk chloride diffusion, modified rapid chloride penetration test (RCPT-10V), and NT Build 492, were conducted to evaluate the performance of these concretes in chloride environments. Additionally, microstructure analyses such as pore structure by nitrogen absorption, pH solution, and XRD analysis were performed to elucidate the performance of the calcined clay-GGBFS blends. The objectives of this study are to assess the impact of precursor composition and alkali activator concentration on chloride resistance and mechanical properties, identify optimal formulations for durability in chloride-rich environments, and evaluate the feasibility of these materials for use in aggressive marine and coastal conditions. The findings will enhance the understanding of the use of calcined clay-GGBFS alkali-activated materials in marine and coastal environments, highlighting their strengths and limitations, and suggesting areas for further research in sustainable

Table 1
Chemical compositions of Calcined clay and GGBFS.

Chemical composition	Low-grade Calcined clay (wt.%)	High-grade Calcined clay (wt.%)	GGBFS (wt.%)
SiO_2	70.42	48.15	31.52
Al_2O_3	22.34	41.63	12.22
Fe_2O_3	2.34	2.27	1.14
CaO	0.49	0.12	44.53
MgO	0.16	0.09	4.62
Na_2O	0.1	0.32	0.21
K_2O	0.19	0.05	0.33
TiO_2	1.1	3.39	1.03
SO_3	0.02	0.09	3.24
Loss on ignition (LOI)	1.76	3.21	0.79

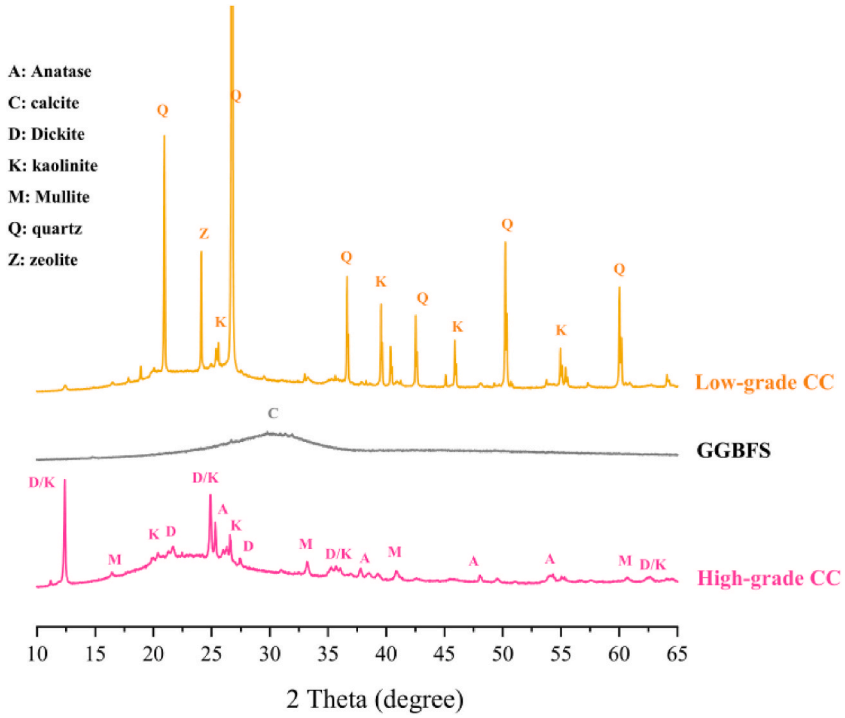

Fig. 1. XRD patterns of Calcined clays and GGBFS.

construction.

2. Materials and methods

2.1. Raw materials

The low-grade calcined clay was obtained from Argeco through industrial flash calcination techniques. This specific type of clay is classified as low-grade due to its kaolinite content accounting for 55 wt% before calcination and 50.9 wt% amorphous contents after calcination. The high-grade calcined clay used in this study was obtained as an industrial product through rotary kiln calcination. The exact kaolinite content of the raw clay before calcination is unknown to the authors, but previous XRD-Rietveld analysis revealed that the calcined clay contained approximately 78.8 wt% amorphous phase [19]. In this study, the calcined clays (both low-grade and high-grade) were used as received from the suppliers without any additional pre-treatment. The GGBFS used in this study originated from Australian Steel Mill Services, located in Port Kembla, New South Wales, Australia. The chemical compositions of calcined clays and GGBFS were measured by X-ray Fluorescence (XRF) (Table 1). Fig. 1 exhibits the crystalline phases of calcined clays and GGBFS, which primarily consist of calcite, quartz, kaolinite, and certain zeolite minerals in the low-grade calcined clay and dickite, mullite, kaolinite, quartz and anatase in the high-grade calcined clay. Fig. 2 shows the particle size distribution of GGBFS and two calcined clays measured by laser diffraction. The alkaline activator for the calcined clay-GGBFS alkali-activated concrete was prepared by mixing sodium silicate solution (Chem-Supply, Port Adelaide SA, Australia - Na_2O = 9.1 %, SiO_2 = 28.9 % and weight ratio (SiO_2:

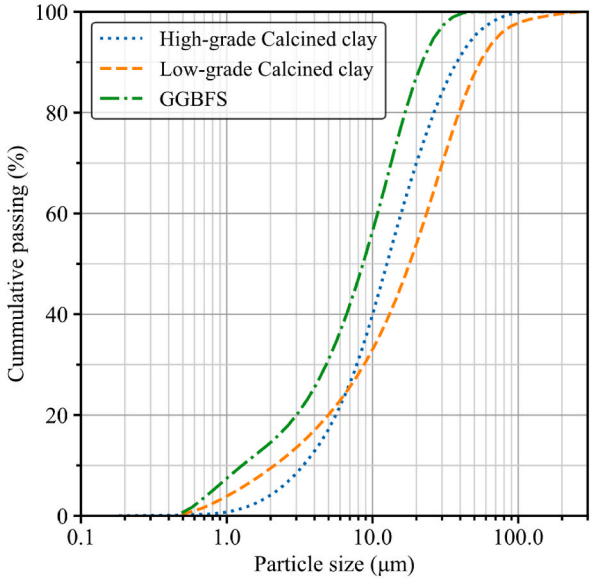

Fig. 2. Particle size distribution (PSD) of calcined clays and GGBFS.

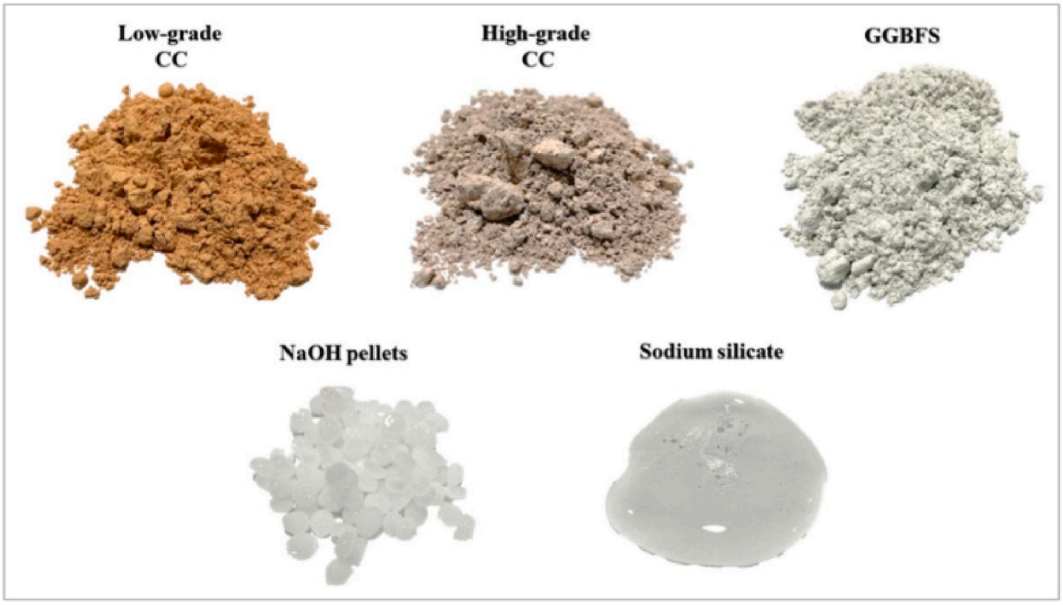

Fig. 3. – Raw precursors and alkali-activated solution materials.

Na_2O) 3.16–3.26) with sodium hydroxide pellets (NaOH) (Ajax Finechem - purity: 98 %, specific gravity: 2.13 g/cm^3, pH: 14) (Fig. 3). The sand has a specific gravity of 2.65 and a water absorption of 3.5 % while the coarse aggregate (10 mm basalt) has water absorption of 1.79 %.

2.2. Alkali-activated concrete mix compositions

The alkali-activated concrete mix was designed according to Table 2. Two distinct types of calcined clay were employed in this investigation, each with varying proportions of amorphous phases. The low-grade calcined clay will be denoted as "LC" while the high-grade material will be referred to as "HC". NaOH pellets and sodium silicate solutions were mixed in proportions to form alkaline solutions in different Na_2O percentages (8 % for the LC only, and 10 % for both calcined clays) and a constant activator silica modulus (Ms = SiO_2/Na_2O molar ratio) equal to 1.5. The activator silica modulus (Ms) of 1.5 was selected for geopolymer concrete containing 70 % calcined clay and 30 % of GGBFS to achieve a suitable compressive strength Indeed, the compressive strength of the same

Table 2
Alkali-activated concrete experimental design mixes.

Mixing [(1)]	GGBFS (%)	Activator modulus (MS)	Activator Concentration $Na_2O\% = Na_2O$/ Binder (%)	Total Binder (Kg/ m^3)	Coarse/Fine aggregate Ratio	Water/Solid [(2)]
70LC/30S-8	30	1.5	8	400	1.9	0.45
70LC/30S-10	30	1.5	10	400	1.9	0.45
70HC/30S-10	30	1.5	10	400	1.9	0.45
50LC/50S-8	50	1.5	8	400	1.9	0.45
50LC/50S-10	50	1.5	10	400	1.9	0.45
50HC/50S-10	50	1.5	10	400	1.9	0.45

*Note 1: LC: Low-grade calcined clay, HC: High-grade calcined clay, S: Ground Granulated Blast-furnace Slag.
*Note 2: Water: free water + water in silicate solution. Solid: Binder + solid in silicate solution (SiO_2 and Na_2O) + NaOH pellet.

Fig. 4. Alkali-activated concrete samples sealed.

concretes with a Ms of 1.0 was too low for chloride environments, as reported in a previous study of the authors [17]. Furthermore, the Ms values higher than 1.5 were not considered in this study to minimize the proportions of sodium silicate solution in the concrete mix compositions, enhancing the sustainability and reducing the environment impacts of alkali-activated materials [20,21]. The alkaline solution for activating the geopolymer concretes was prepared by dissolving sodium hydroxide (NaOH) pellets in water to achieve the desired molarity. The NaOH solution was allowed to cool to room temperature before being mixed with sodium silicate solution in a specific ratio to form the final alkaline activator. The alkaline solution was prepared 24 h prior to usage. The samples were mixed in an electric Pan-drum mixer. Afterwards, fresh concrete was poured into different moulds and vibrated on a vibrating table to remove entrapped air. After 1 day, all concrete samples were demoulded, sealed and transferred to a controlled room with a temperature of 23 ± 2 °C.

3. Experimental program

3.1. Compressive strength

The 28-day compressive strength of the alkali-activated concretes made with calcined clay and GGBFS was evaluated using three-cylinder samples with a diameter of 100 mm and a height of 200 mm, in compliance with ASTM C39 standards [22]. A UH-500kN XR Universal Hydraulic Test Frame was utilized for the compression tests. After being cast, the samples were sealed and wrapped (Fig. 4), then cured for a 28-day period in a regulated environment with a stable temperature of 23 ± 2 °C and a relative humidity of 55 %, before undergoing testing.

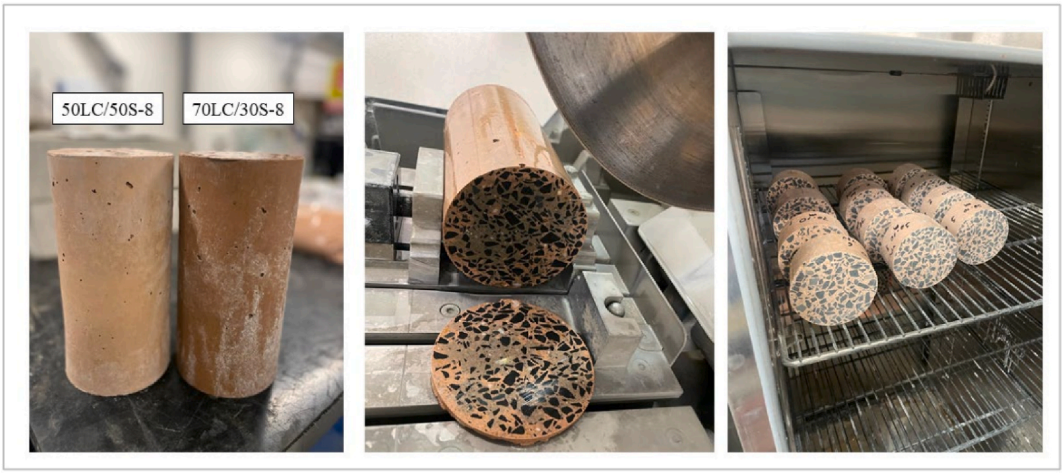

Fig. 5. Discs specimens subjected to water absorption and VPV tests.

3.2. The water absorption and volume of permeable voids (VPV)

The disc specimens, measuring 100 mm in diameter and 50 mm in thickness, were subjected to water absorption and VPV tests. These discs were obtained by cutting standard cylinders, ensuring that the sampling location was at least 25 mm away from both ends of the cylinders. Prior to testing, the samples underwent a drying process in an oven set at a temperature of 105 °C for approximately 48 h or until there was no significant change in weight (mass change <0.5 %) within a 24-h period (Fig. 5). The measurement of water absorption and VPV after a curing period of 28 days was performed using ASTM C642 guidelines [23].

3.3. Surface and bulk resistivity

Surface and bulk resistivity measurements were taken at the 28-day mark using a Proceq Resipod resistivity meter. Water-vacuum-saturated cylindrical samples, sized 100 × 200 mm, were used for the tests. A four-pin Wenner probe array extension attached to the Proceq Resipod device was employed to evaluate the surface resistivity of the samples. The distance between the electrodes on the extension was fixed at 50 mm. Each sample underwent twelve measurements, spaced out at 90° intervals around the specimen [24]. Bulk electrical resistivity was assessed with the same Proceq Resipod device, utilizing two stainless steel base plates for contact. This methodology aligns with techniques described by Noushini and Castel [25].

3.4. Chloride diffusion tests

The chloride diffusion resistance tests, including bulk chloride diffusion, modified-RCPT, and NT Build 492, were conducted following the standard procedures outlined in relevant guidelines. The results were compared to threshold values provided in the respective standards (e.g., ASTM C1202 for RCPT and NT Build 492) and performance-based criteria for alkali-activated concretes in chloride environments proposed in previous studies [1,26,27]. This approach ensures the reliability of our findings in the context of existing durability criteria and standards.

3.4.1. Rapid chloride penetration test (RCPT) – modified

To assess the concrete's ability to resist chloride ion penetration, a modified RCPT using a 10V voltage was employed, as suggested by Noushini & Castel [26]. The standard 60V voltage from the RCPT-ASTM C1202 protocol was avoided because the high conductivity of the specimens led to overheating issues [26]. Following a curing period of 28 days, three identical companion specimens were subjected to the modified-RCPT 10V. The tested samples had dimensions measuring 50 mm in thickness and 100 mm in diameter.

3.4.2. Rapid migration test (RMT) - NT BUILD 492

To assess the non-steady-state chloride migration coefficient, the test was performed according to the Nordtest NT Build 492 protocol [28]. The specimens were 50 mm thick concrete discs, extracted from the central section of three identical 100 × 200 mm cylinders after a 28-day curing period. The experiment used a catholyte solution of 10 % NaCl in tap water and an anolyte solution of 0.3N NaOH in distilled water. An electrical potential between 10V and 60V was applied to induce chloride ions to migrate into the concrete specimen. After a set period, ranging from 6 to 24 h, the specimen was axially divided into two parts. To determine the chloride penetration depth, each half was sprayed with a 0.1 mol/L $AgNO_3$ solution on the fractured surface. The non-steady-state migration coefficients were then calculated according to NT Build 492 guidelines [28].

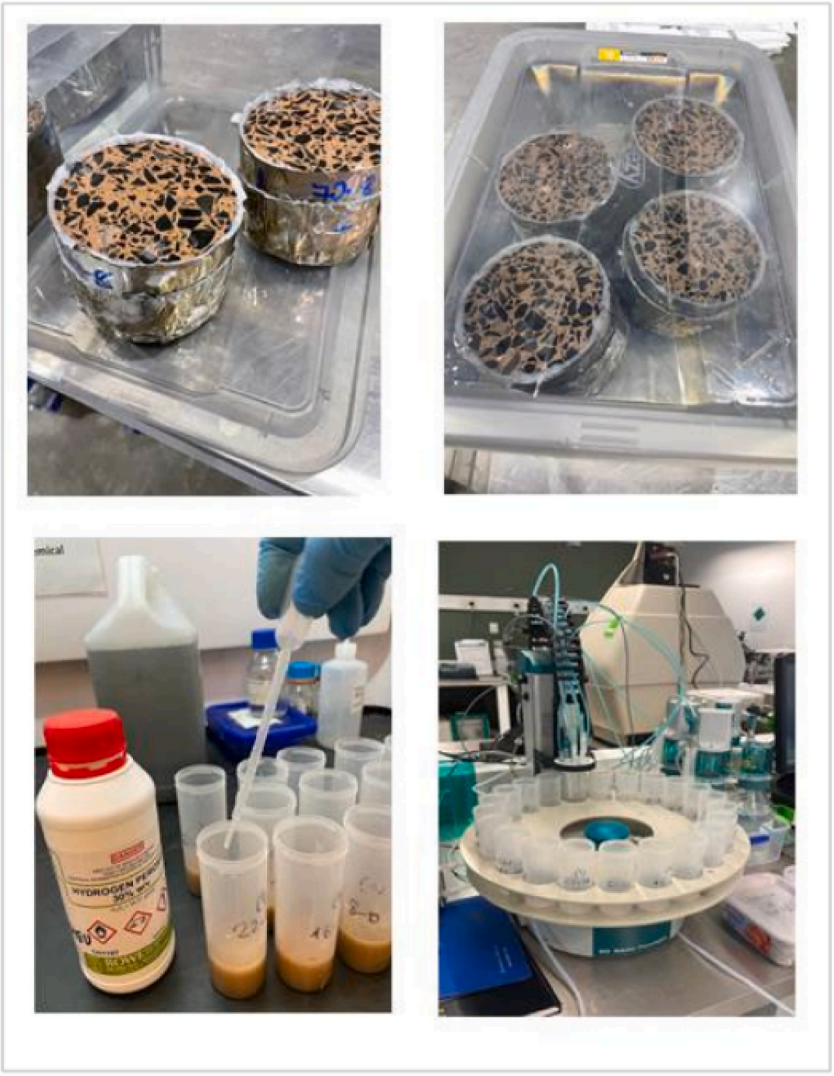

Fig. 6. Bulk Diffusion samples and chloride content analysis by titration.

3.4.3. Bulk diffusion test

The bulk diffusion assessment was carried out based on the ASTM C1556 protocol [29]. After a 28-day curing period, alkali-activated concrete cylinders were sliced into discs measuring 100 mm in diameter and 75 mm in height. These discs were then vacuum-saturated with water and, after a 24-h soaking period, all sides were sealed with self-adhesive film except for the surface that would be exposed to the sodium chloride solution. The discs were vacuum-saturated once more before being submerged in a 165 g/L NaCl solution for 35 days (Fig. 6). At the end of this exposure period, samples of concrete powder were collected at 1 mm intervals from the exposure surface to a depth of 25 mm using a profile grinder. These samples were individually stored in plastic vials for subsequent analysis of their chloride content. The acid-soluble chloride content in the alkali-activated concrete powder was quantified using ASTM C1152 methodology with a potentiometric titration machine and expressed as a mass percentage of the concrete powder [30]. The apparent chloride diffusion coefficients were calculated by using non-linear regression method from chloride profiles against exposure depth.

3.5. Pore structure by N_2 adsorption

The pore size distribution and level of porosity in the hardened alkali-activated pastes were evaluated after 28 days of curing. The compositions used for testing followed proportions as outlined in Table 2, without the presence of coarse and fine aggregate. The alkali-activated pastes were prepared under controlled conditions and cured for a period of 28 days. Before conducting the experiment, the paste samples underwent immersion in isopropanol to halt hydration, followed by vacuum-drying at a temperature of 40 °C for half an hour [31]. Crushed and ground samples were utilized and then screened using a sieve with a particle size of 75 μm. Approximately 1

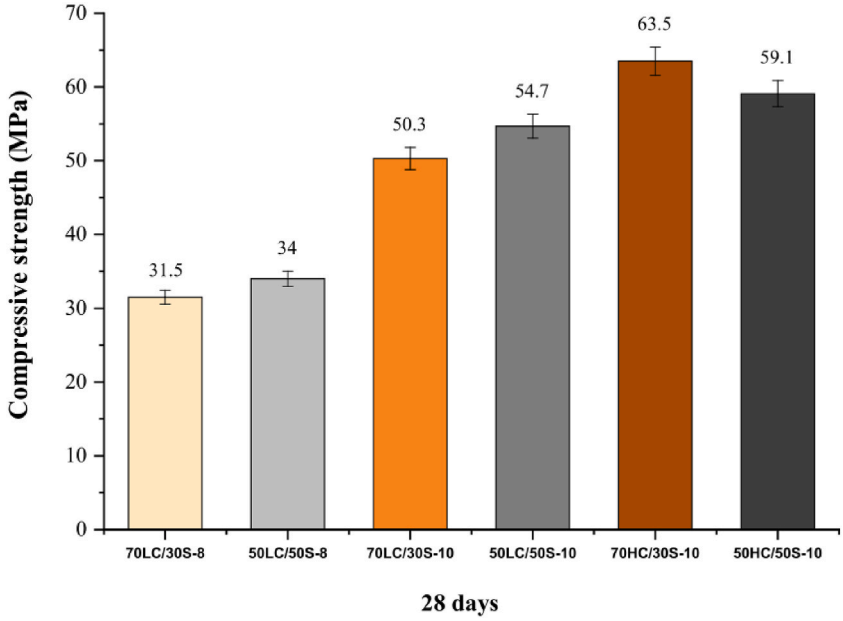

Fig. 7. Compressive strength of alkali-activated Calcined clay/GGBFS concrete blend.

g of sample was used for the analysis. To assess the distribution of pore sizes, the nitrogen adsorption technique was utilized. The pore size distributions (PSDs) of the samples were calculated using the Barrett-Joyner-Halenda (BJH) method with the Kelvin model of pore filling.

3.6. pH measurement

The pH level of the hardened alkali-activated pastes was analyzed after 28 days of curing. The samples were divided into two categories, pre-exposure; related to samples with 28 days curing and samples exposed to 165 g/L NaCl solution for 35 days (same conditions as the samples exposed to the bulk diffusion section 3.4.3). To conduct this analysis, the samples were crushed and ground to a particle size smaller than 75 μm by passing through a sieve. Paste mixes were prepared according to the proportions specified in Table 2, but without including any aggregate. These ground paste samples were then dispersed in distilled water at a ratio of 1:1 and mixed for a duration of 5 min [32,33]. The pH value was measured using a pH meter with an accuracy level of ±0.01 and three separate measurements were taken.

3.7. XRD analysis

The mineralogical composition of the composite material was assessed through XRD analysis. A Bruker D8 Discover diffractometer was used to examine a finely powdered paste derived from samples that had been aged for 28 days (pre-exposure) and samples exposed to 165 g/L NaCl solution for 35 days (same conditions as the samples exposed to the bulk diffusion section 3.4.3). The XRD measurements were carried out at standard settings with an electrical current of 20 mA and voltage of 40 kV. Scanning took place over a range of angles (2θ) spanning from 5° to 80°, however only the 20°–65° 2θ was studied.

4. Results and discussion

4.1. Compressive strength

The compressive strength of the concrete produced using alkali-activated calcined clay and GGBFS were assessed after being sealed and cured at a temperature of 23 ± 2 °C for a period of 28 days. The results, as shown in Fig. 7, demonstrate that the calcined clay-GGBFS geopolymer concretes achieved an average compressive strength ranging from 31.5 to 63.5 MPa. This level of performance qualifies them for various structural applications, including chloride environment. Both the increased alkaline concentration and variations in types of calcined clay showed varying effects on compressive strength. The analysis was conducted by categorizing the data based on the ratio of calcined clay and GGBFS precursors used. In addition, the compressive strength results of alkali-activated calcined clay and GGBFS concretes in this study are comparable to other alkali-activated concretes containing fly ash or GGBFS as well as OPC-based concretes with calcined clay to be used in chloride environments [27,34]. Noticeably, all concretes with 10 % Na_2O concentration exhibited a higher compressive strength than alkali-activated concretes with 100 % GGBFS [35].

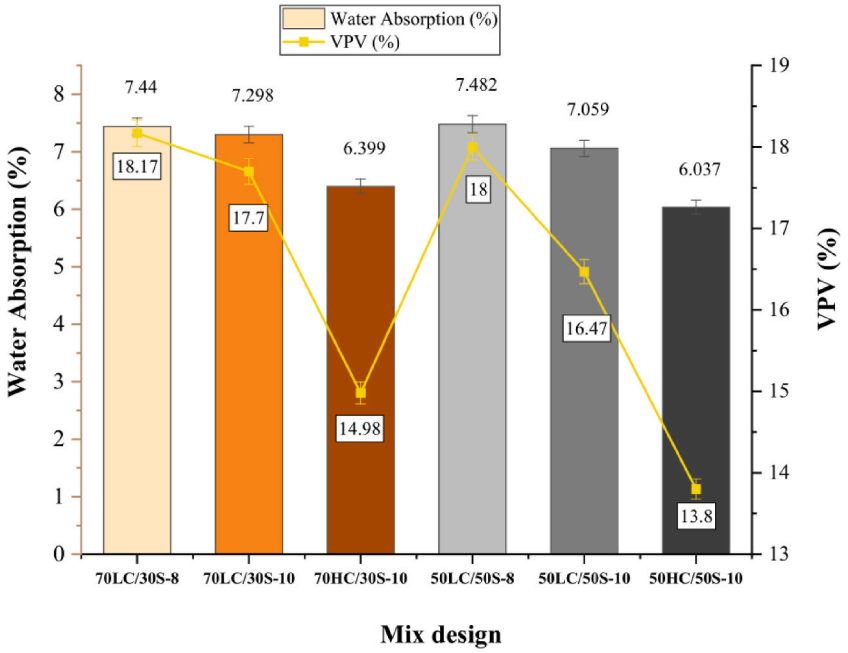

Fig. 8. Water absorption and volume of permeable voids (VPV) of alkali-activated Calcined clay/GGBFS concrete.

For the samples containing 70 % calcined clay and 30 % GGBFS (70CC30S group), it is evident that the mixture with the high-grade calcined clay and 10 % Na_2O% (70HC30S-10) exhibited the highest compressive strength at 63.5 MPa. On the other hand, the lowest compressive strength was observed for the mixture consisting of the low-grade calcined clay and Na_2O% of 8 %, reaching 31.5 MPa at 28 days. A similar trend was observed in the 50CC50S group (Fig. 7), where the highest compressive strength of 59.1 MPa was achieved by the sample 50HC/50S-10, while samples 50LC/50S-8 and 50LC/50S-10 obtained compressive strengths of 34 MPa and 54.7 MPa respectively. It is worth noting that when comparing samples activated with the same 10 % Na_2O, replacing low-grade calcined clay with high-grade calcined clay had a more significant impact on samples containing 70 % calcined clay. The sample 70HC30S-10 showed an increase in compressive strength of almost 20.78 %, compared to 70LC30S-10. However, this difference was only about 7.44 % within the 50CC50S group. The increase can likely be attributed to a larger concentration aluminosilicates and amorphous phases in the high-grade calcined clay compared to low-grade ones.

4.2. The water absorption and volume of permeable voids (VPV)

The water absorption and the volume of permeable voids (VPV) were measured in order to assess the transport properties of the alkali-activated concrete specimens. Fig. 8 illustrates the results for water absorption. When using HC-calcined clay in the blends 70HC30S-10 and 50HC50S-10, the water absorption was approximately 6.4 % and 6.0 % respectively. In contrast, when LC-calcined clay was mixed with GGBFS at the same alkaline solution concentration of 10 % (70LC30S-10 and 50LC50S-10), their water absorption increased to around 7.3 % and 7.05 %, respectively. The samples activated with concentration 8 % and LC-calcined clay showed the highest water absorption, these being 7.44 % and 7.48 % for 70LC30S-8 and 50LC50S-8, respectively.

The volume of permeable voids (VPV) shows similar patterns to water absorption results, although a larger discrepancy is noticeable when the alkaline activator concentration and the amorphous phases are increased (Fig. 8). For the group using 70 % calcined clay (70LC30S), the samples 70LC30S-8 and 70LC30S-10 showed VPV results of 18.17 % and 17.7 % respectively when LC-calcined clay was used, indicating that increasing alkaline concentration from 8 to 10 % led to a reasonable reduction in permeable void volume. However, when high-grade calcined clay was used at the same concentration of 10 %, the reduction in permeable void volume (as observed in sample 70HC30S-10) was even more significant, reaching approximately around 14.98 %. Similar results were noticed in the category containing 50 % calcined clay, where samples 50LC50S-8 and 50LC50S-10 exhibited absorption rates of approximately 18 % and 16.47 %, respectively. 50HC50S-10 concrete displayed the lowest absorption rate among all tested samples at around 13.8 %. VPV values of all calcined clay-GGBFS alkali-activated concretes were lower than that of 100 % GGBFS specimens achieving 21.2 % [36]. The improved performance of the samples using HC-calcined clay aligns with the findings from compressive strength tests, where a higher proportion of amorphous and reactive phases in the HC-calcined clay resulted in increased dissolution of aluminosilicates, leading to less permeable and more dense concrete structures.

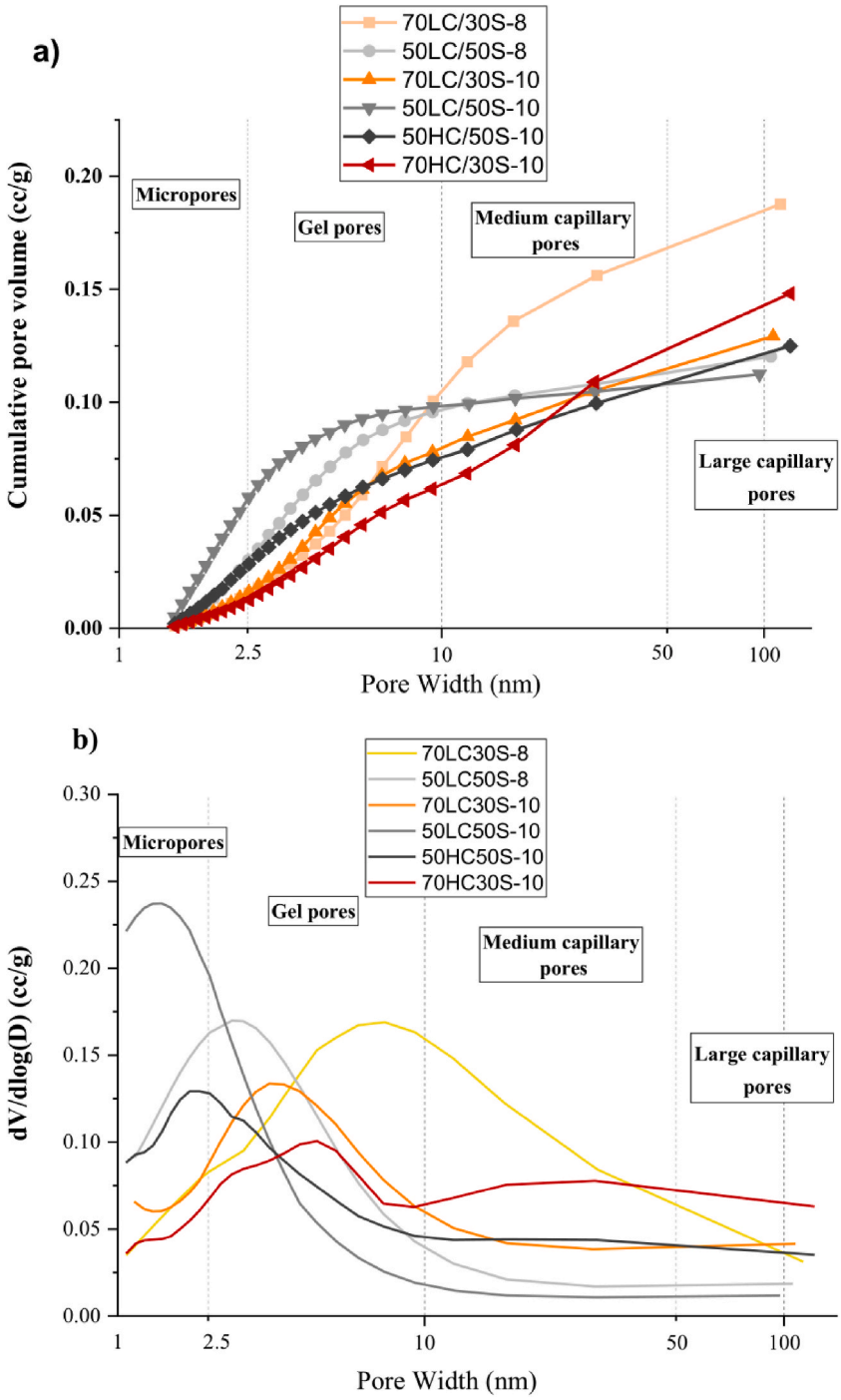

Fig. 9. Pore size distribution of alkali-activated calcined clay/GGBFS pastes determined by nitrogen adsorption and BJH method. a) cumulative pore volume b) differential pore distribution.

4.3. Pore structure study by N_2 adsorption

The pore characteristics, such as porosity, distribution of pore sizes, continuity, and tortuosity play a key role in determining the chloride transport properties of both ordinary Portland cement and alkali-activated materials. Typically, samples with lower overall porosity, smaller pores, limited connectivity between pores, and more convoluted pathways exhibit higher resistance to chloride ingress [6]. Pore sizes can be divided into various categories: micropores, small capillary or gel pores, medium capillary pores, and large capillary pores. Micropores range in size from 0.5 nm to 2.5 nm, while small capillary or gel pores fall within the 2.5 nm–10 nm

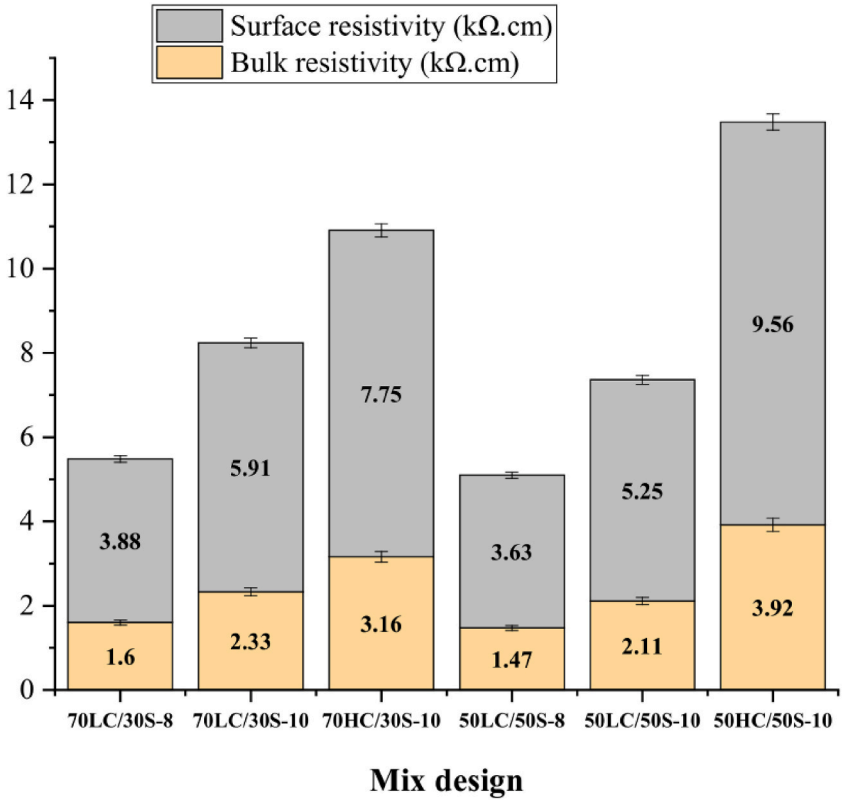

Fig. 10. Surface and bulk resistivity of Alkali-activated concrete after 28 days.

range. Medium capillary pores have sizes ranging from 10 nm to 50 nm, and large capillary pores measure between 50 nm and 10 μm [37].

The pore size distribution of alkali-activated calcined clay/GGBFS pastes after a 28-day curing period is shown in Fig. 9(a). The analysis revealed that variations in the precursor proportions, Na_2O% concentrations, and type of calcined clay had distinct impacts on the pore size distribution of alkali-activated concretes. Notably, mixtures with a high content of GGBFS (50CC50S group) showed significant changes. Fig. 9 (a) demonstrates that the mix 50LC50S-10 had higher concentrations of micropores and gel pores compared to other samples such as 50LC50S-8 or even the high-grade calcined clay sample (50HC50S). However, it is important to note that the 50HC50S sample had a smaller cumulative pore volume than samples with similar precursor ratios but different types of calcined clay and lower Na_2O% concentrations. This indicates that the dissolution processes associated with HC-calcined clay resulted in a denser and more refined pore structures for these particular samples. Meanwhile, the blends consisting of 70 % calcined clay (referred to as the 70CC30S group) showed similar concentrations of micropores and gel pores for the low-grade calcined clay samples (70LC30S-8 and 70LC30S-10) (Fig. 9(a)). In contrast, the samples made with high-grade calcined clay (70HC30S-10) had fewer gel pores in comparison. Much like the observations in the 50 % calcined clay and 50 % GGBFS, the mixture that included high-grade calcined clay yielded a smaller overall pore volume. On the other hand, the 70LC30S-8 sample had the highest total pore volume among all the tested blends.

Fig. 9(b) displays the differential pore distribution curves for the six mixtures. The critical pore diameter, indicated by the highest peak in these curves, is widely recognized as a significant factor affecting the permeability and diffusion properties of conventional cement materials [38]. Based on the analysis findings, it was determined that the pore diameters critical to the materials 70LC30S-8, 70LC30S-10, 70HC30S-10, 50LC50S-8, 50LC50S-10 and 50HC50S-10 are approximately 7.4 nm, 3.84 nm, 4.9 nm, 3 nm, 1.79 nm and 2.28 nm respectively. The largest pore diameter, 7.4 nm, in the 70LC30S-8 mix aligned with the highest cumulative pore volume shown in Fig. 9 (a). However, while 70LC30S-10 and 50HC50S-10 exhibited similar cumulative pore volume curves, as presented in Fig. 9 (a), the critical pore diameter of 3.84 nm in 70LC30S-10 was considerable higher than the 2.28 nm diameter in 50HC50S-10 mix. Similarly, the 50LC50S-8 mix presented higher critical pore diameter than 50LC50S-10 mix, although both mixes exhibited comparable total cumulative pore volume beyond 100 nm. Therefore, both cumulative pore volume and critical pore diameter should be considered when evaluating the effects of pore structures on the chloride diffusion resistance of alkali-activated calcined clay-GGBFS concretes.

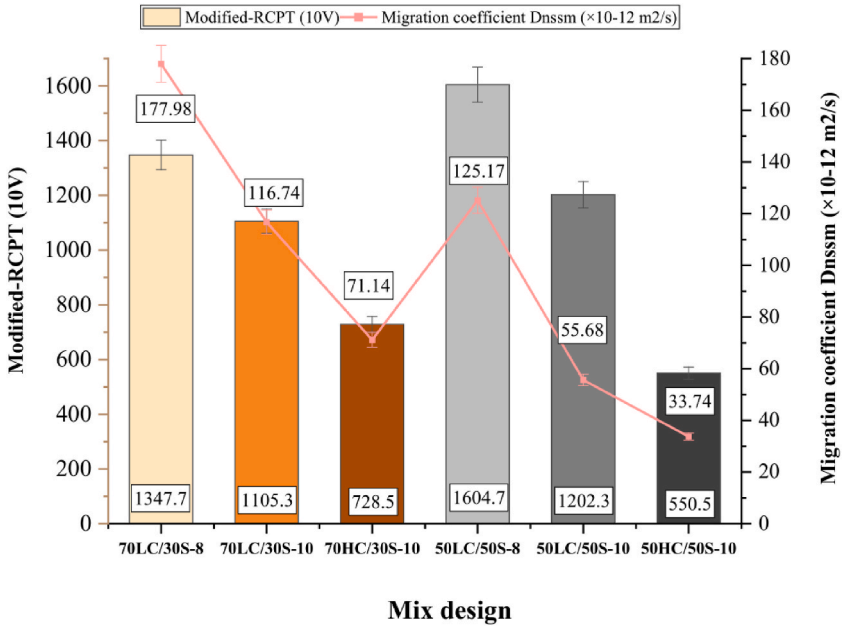

Fig. 11. – Modified-RCPT (10V) and non-steady-state migration coefficient (D_{nssm}) of alkali-activated concretes.

4.4. Surface and bulk resistivity

Concrete resistivity is commonly used to measure its ability to withstand the penetration of aggressive ions such as chloride [39]. It serves as an indicator of concrete's resistance against the flow of ions in the pore solution. Concrete with lower porosity and higher tortuosity restricts the movement of ions such as Na^+, K^+, and OH^- in the pore solution [25]. Therefore, higher electrical resistivity suggests reduced permeability, while lower electrical resistivity indicates greater permeability. The presence of metallic ions in large quantities also negatively affects the resistivity by reducing it [38,39].

According to the findings presented in Fig. 10, it is evident that increasing concentrations of Na_2O% and the amorphous phases in calcined clays contribute to higher electrical resistivity in alkali-activated concrete samples. The LC-calcined clay showed bulk resistivity values of 1.6 kΩcm and 2.33 kΩcm for the 70LC30S-8 and 70LC30S-10 mixtures respectively, while the corresponding surface resistivity values were found to be 3.88 kΩcm and 5.91 kΩcm. Additionally, within this group, the highest bulk (3.16 kΩcm) and surface (7.75 kΩcm) resistivity values were obtained by using a high-grade calcined clay (70HC30S10), which can be attributed to its increased dissolution rate leading to a denser microstructure as observed from porosity results; hence limiting ion movement within the pore solution. Fig. 10 illustrates a similar trend for the 50CC50S group. Bulk resistivity values of 1.47 kΩcm and 2.11 kΩcm were obtained for 50LC50S-8 and 50LC50S-10, respectively, while the corresponding surface resistivity values were found to be 3.63 kΩcm and 5.25 kΩcm. Among all groups tested, it was observed that the best performance in terms of both bulk and surface resistivity was exhibited by the concrete mixture with a high-grade calcined clay (i.e., 50HC50S), which recorded values of approximately 3.92 kΩcm and 9.56 kΩcm, respectively. The highest surface and bulk resistivity results of 70HC30S-10 and 50HC50S-10 were consistent with the lowest water absorption and VPV values as presented in Fig. 8. This can be attributed to a lower porosity and less interconnected pores when using high-grade calcined clay, restricting the ions movement and increasing the resistivity.

When comparing the performance of two groups with varying percentages of precursor, it was observed that samples containing a higher proportion of low-grade calcined clay (70LC30S-8 and 70LC30S-10) showed a slight improvement in both bulk and surface resistivity comparing to the 50LC50S-8 and 50LC50S-10 samples, regardless of Na_2O concentration. However, when using HC-calcined clay, the opposite trend was observed. The sample 50HC50S-10 exhibited superior performance compared to the 70HC30S-10 sample. This phenomenon may be linked to the free ions in the solution portion of these specimens along with the predominant phases in these samples (N-A-S-H or C-A-S-H), mainly in the samples with low grade calcined clay that presented smaller reactive phases before alkali activation.

4.5. Modified -RCPT (10V) and rapid migration test (RMT) - NT BUILD 492

In order to assess the chloride permeability/migration of OPC materials, the most commonly used tests are RCPT and NT BUILD 492. These tests have gained popularity due to their shorter testing duration, with RCPT taking approximately 6 h and NT BUILD 492 ranging from 6 to 96 h [6]. To measure the chloride penetration resistance of alkali-activated concrete mixes, an RCPT test (modified with 10V) was performed, and the results of the RCPT test are shown in Fig. 11. The observed Coulomb charges for the mixtures 70LC/30S-8, 70LC/30S-10, 70HC/30S-10, 50LC50S-8, 50LC50S-10 and 50HC50S-10 were recorded at values of 1347.7, 1105.3,

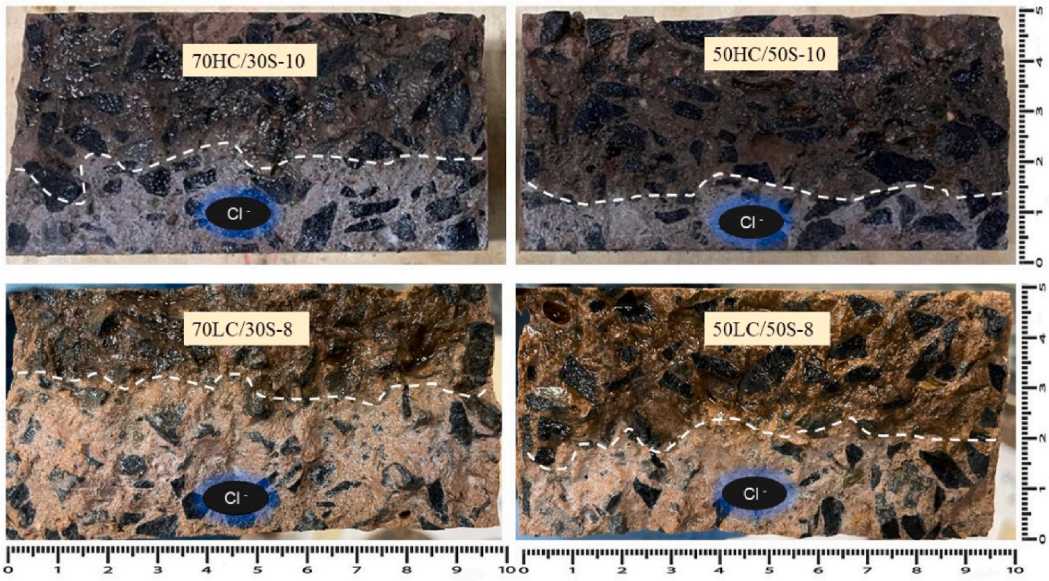

Fig. 12. Chloride Penetration Depth measurement after conducting NT Build 492; VOLTGE = 10–20V.

728.5, 1604.7, 1202.3 and 550.5 Coulombs, respectively. In terms of performance evaluation among the tested specimens, the mixtures incorporating HC-calcined clay (70HC/30S-10 and 50HC/50S-10) exhibited superior behavior. By comparing formulations containing LC-calcined clays, it is observed that an increase in Na_2O% leads also to a reduction in charge passing across the sample. An additional observation can be made by comparing the performance of two groups with varying percentages of precursor materials. It was found that samples containing a higher proportion of low-grade calcined clay (70LC30S-8 and 70LC30S-10) exhibited lower charge passed (1347.7 and 1105.3 Coulombs, respectively) compared to the 50LC50S-8 and 50LC50S-10 samples (1604.7 and 1202.3 Coulombs, respectively), regardless of Na_2O concentration. This behavior can be attributed to the higher content of N-A-S-H gel in samples with a greater proportion of low-grade calcined clay, which consumes more free alkalis, thereby reducing the ionic conductivity in the pore solution [26]. Consequently, these samples demonstrated reduced charge transfer during the modified RCPT (10V), highlighting their improved resistance to chloride ion penetration. However, when HC-calcined clay was used, the opposite trend was observed. The sample with a ratio of 50HC50S-10 demonstrated superior performance compared to the sample with a ratio of 70HC30S-10 (Figs. 11 and 12). These findings align with both bulk and surface resistivity results (Fig. 10) and raise questions about how pore solution and free ions may be influencing these outcomes. The observed outcomes may be linked to the existence of unbound ions (such as Na^+ and OH^-) in the pore solution. Previous studies have indicated that the addition of larger quantities of the same low-grade calcined clay resulted in a higher production of N-A-S-H, leading to increased consumption of Na^+ from the pore solution [17]. According to Bernal, de Gutiérrez & Provis, decreasing the concentration of Na^+ ions in the pore solution can result in a reduction of the charge passed in the RCPT test [40]. The presence of sodium ions in the pore solution causes counter-diffusion as chloride ions are electrically transported through the pore network by the applied electrical field gradient, leading to an increase in the amount of charge transferred.

Fig. 11 also presents the non-steady-state migration coefficient of all concrete mixes. The D_{nssm} values ranged from 33.74 to 177.98 ($\times 10^{-12}$ m^2/s). Among the samples containing an equal proportion of calcined clay and GGBFS, the highest chloride diffusion resistance was achieved by using HC-calcined clay in a mixture ratio of 50HC50S-10, resulting in a D_{nssm} value of 33.74 ($\times 10^{-12}$ m^2/s). Conversely, when LC-calcined clay was used with Na_2O concentrations at both 8 % and 10 %, results were obtained at values of approximately 55.68 and 125.17 ($\times 10^{-12}$ m^2/s) respectively. Similarly, the performance of mixtures with 70 % calcined clay was found to be better when the concentration of LC-calcined clay was increased to 10 %, and when the less reactive LC-calcined clay was substituted with more reactive calcined clay. 70LC/30S-8, 70LC/30S-10 and 70HC/30S-10 presented D_{nssm} values of 177.98, 116.74 and 71.14 ($\times 10^{-12}$ m^2/s) respectively.

The comparisons between the groups with different proportions of precursor reveal conflicting results when examining NT Build 492 and modified-RCPT 10V. The D_{nssm} findings indicate that the group utilizing a mixture of 50 % calcined clay and 50 % GGBFS performed better in terms of chloride migration compared to the group using 70 % calcined clay, despite having the same alkaline concentration and type of calcined clay. Conversely, RCPT showed an opposite trend, except for cases involving high-grade calcined clay. These contradictory findings can be attributed to a higher concentration of ionic solution used to activate the geopolymer concrete, which led to increased conductivity and charge passed. This finding suggests that the resistance of geopolymer concrete to chloride ion diffusion is influenced by various factors, including concentration and composition rather than solely its structural properties. It indicates that the alkali concentration and composition of free ions in the pore solution have a significant impact on both RCPT and resistivity tests, as these tests measure conductivity instead of directly measuring chloride ion migration [2].

Table 3
Performance-based requirements for geopolymer concrete in Chloride environment proposed by Noushini & Castel [26] and Noushini, Nguyen & Castel [27].

Exposure classification (AS 3600)	Minimum Strength (MPa)	Charge passed ASTM C1202 (Coulombs)	Charge passed modified ASTM C1202[a] (Coulombs)	Chloride migration coefficient – NT Build 492[b] ($\times 10^{-12}$ m^2/s)	Chloride diffusion coefficient ASTM C1556 ($\times 10^{-12}$ m^2/s)	Chloride penetrability
–	–	>4000	≥350	≥13.5	≥16.0	High
B1	35	2000–4000	220–350	<13.5	6.0–16.0	Medium
B2	40	1000–2000	120–220	<5.0	3.0–6.0	Low
C1 and C2	40	<1000	<120	<2.5	<3.0	Very Low

[a] Modified ASTM C_{1202}: applied voltage 10V, test duration 6h. Proposed by Noushini & Castel [26].
[b] Correlation with ASTM C1556 proposed by Noushini, Nguyen & Castel [27].

Table 4
Apparent chloride coefficient of alkali-activated concretes after 35 days in saline solution.

Apparent chloride coefficient - Bulk diffusion ($\times 10^{-12}$ m^2/s)	
70LC/30S-8	355.9 ± 99.2
70LC/30S-10	104.84 ± 67.76
70HC/30S-10	42.29 ± 12.78
50LC/50S-8	318.9 ± 16.1
50LC/50S-10	71.78 ± 37.07
50HC/50S-10	27.0 ± 2.90

4.6. Performance-based criteria using modified-RCPT, NT build 492 and correlations with ASTM C1556 and AS 3600

AS 3600-2009 includes four exposure classifications (B1, B2, C1, and C2) that address chloride contamination concerns. Each classification specifies necessary precautions to prevent corrosion of reinforcement due to chloride exposure. These measures may include minimum concrete cover, minimum characteristic compressive strength, as well as some supplementary protective techniques. Exposure classification B1 is suitable for areas located near the coast, specifically within a range of 1 km–50 km from the coastline. On the other hand, exposure classification B2 applies to coastal zones situated within 1 km of large saltwater bodies and also includes permanently submerged surfaces such as maritime structures in sea water. Exposures C1 and C2 are designated for the surface of maritime structures that come into direct contact with sea water in spread and tidal zone [26,41].

Currently, there is no specific standard in Australia for alkali-activated concretes or geopolymers. To address this issue, a performance-based approach was proposed by Noushini and Castel, which involved the creation of an extensive database that includes chloride diffusivity values for both alkali-activated concrete and OPC concretes based on ASTM C1556 (bulk diffusion test) [26,29]. This data was then correlated with a modified version of RCPT (10V), leading to recommendations and correlations with AS 3600 guidelines (Table 3). Based on AS 3600 recommendations and criteria, only four of the alkali activated concretes (70LC30S-10, 70HC30S-10, 50LC50S-10 and 50HC50S-10) in this research achieved the minimum average compressive strength (B1 exposure-35 MPa) for concrete exposed to marine environments (Table 3). However, according to Noushini and Castel proposal, none of these concretes should be used in chloride environments since all concrete results were higher than 350 Coulombs [26].

Another performance-based specification was proposed by Noushini, Nguyen & Castel, relating to the chloride migration coefficient (NT Build 492) and chloride diffusion coefficient (ASTMC1556) specifically for geopolymers and alkali-activated concrete (Table 3) [27–29]. Based on Noushini, Nguyen & Castel recommendations, none of the mixes in this study should be exposed to chloride environments as all mixes had a non-steady-state migration coefficient (D_{nssm}) higher than 13.5($\times 10^{-12}$ m^2/s), characterizing these concretes as high-chloride penetrability [27]. However, the relationship between chloride migration tests and chloride diffusion coefficients proposed in their study has only been established using a limited amount of experimental data. To determine the accuracy of this proposed method, a more comprehensive database is needed that incorporates results from Bulk diffusion- ASTM C1556 tests, which better simulate real chloride environments.

4.7. Apparent chloride coefficient - bulk diffusion- ASTM C1556

In contrast to the RCPT and NT Build 492 tests, the ASTM C1556 chloride diffusion tests (also known as bulk diffusion test) is the most reliable for replicating real-world conditions. Before performing the chloride diffusion test, all specimen surfaces (except the one exposed) are sealed to allow only one-dimensional diffusion. This bulk diffusion test involves submerging the sample in a high-concentration NaCl solution (165 ± 1 g/L). Although this NaCl concentration significantly exceeds the typical salinity of seawater, which is about 3.5 %, the duration of the test can be reduced to just 35 days [6]. The calculated apparent chloride diffusion coefficients (D_a) for all alkali-activated concretes are outlined in Table 4 Notably, the low-grade calcined clay samples, specifically 70LC30S-8 and

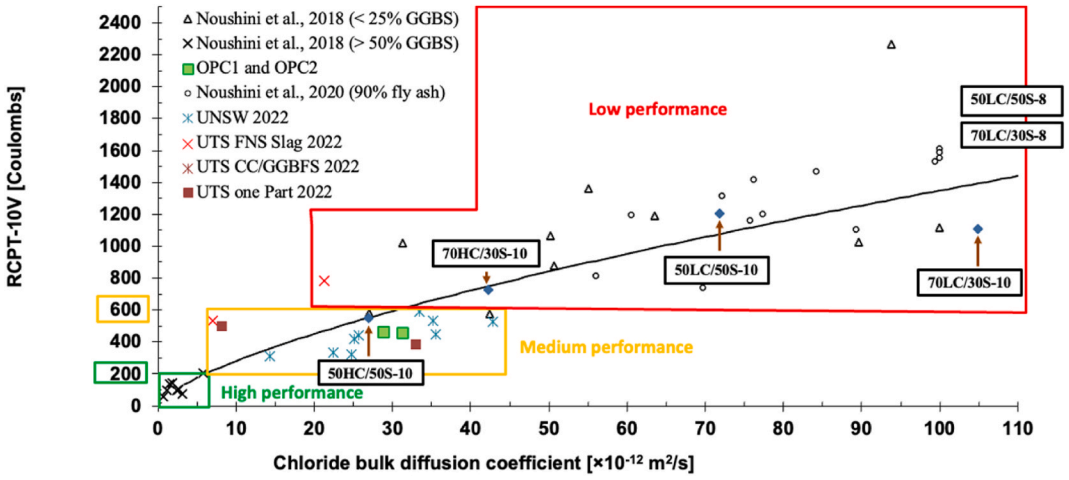

Fig. 13. Performance-based classification of geopolymer concretes based on modified-RCPT and Bulk diffusion test [1].

50LC50S-8, with an 8 % Na_2O activator concentration, exhibited exceptionally low resistance to chloride diffusion. These samples displayed extremely high diffusion coefficients, with values such as D_a over 300 $\times$ 10^{-12} m^2/s), indicating poor performance in resisting chloride penetration. When the activator concentration of Na2O for the same low-grade calcined clay was increased to 10 %, a significant decrease in chloride diffusion was observed. Specifically, the samples labeled 70LC30S−10 and 50LC50S−10 showed much lower apparent chloride diffusion coefficients, approximately 104.84 and 71.78 ($\times 10^{-12}$ m^2/s), respectively. This indicates that elevating the activator concentration effectively improved the material's resistance to chloride diffusion penetration. In Babaee & Castel study involving fly ash mixed with GGBFS, there was a notable trend: as the alkaline concentration increased (from 5 % to 8 %), there was a corresponding rise in the chloride diffusion coefficient [42]. This led to a decline in performance compared to samples with lower Na_2O%. Interestingly, this observation contrasts with the findings from our research, which showed an opposite trend.

When high-grade calcined clay was used, the decline in the apparent chloride diffusion coefficient (D_a) was even more significant. Specifically, samples 70HC30S-10 and 50HC50S-10 showed D_a values around 27 and 42.29 ($\times$ 10^{-12} m^2/s) respectively. This suggests that using high-grade calcined clay with a higher activator concentration can greatly enhance the material's resistance to chloride ingress. These values are similar to the values found by Noushini & Castel for OPC grade 50–60 MPa compressive strength [26]. This similarity suggests a comparable level of performance. Clearly, the inclusion of GGBFS had a marked effect on the performance to the chloride diffusion, similar to the NT Build 492 results (Fig. 10). Samples containing a higher proportion of GGBFS demonstrated enhanced resistance to chloride diffusion. This improvement is likely related to the calcium-rich phases provided by GGBFS, which contribute to lower ion mobility and microstructure densification, as corroborated by the results of the porosity tests. Noushini & Castel reported that a minimum of 50 % GGBFS was necessary to reach an acceptable level of resistance against chloride diffusion [26]. Nonetheless, it was observed that only mixtures containing more than 75 % GGBFS exhibited properties compatible with conditions of severe chloride exposure.

Fig. 13 illustrates the outcomes from both the bulk diffusion test and the modified RCPT-10V, plotted according to the classification suggested by Nguyen et al. [1]. Overall, the modified-RCPT results correlate well with the bulk diffusion test results regardless the alkali-activated concrete mixes. The proposed performance can be classified into three distinct categories based on the charge passed through the material: High performance is attributed to samples with charge transfer of 200 Coulombs or less; Medium performance is designated for those with charge passing greater than 200 Coulombs but less than 600 Coulombs; and Low performance is tagged to samples with a charge exceeding 600 Coulombs.

The 70LC30S-8 and 50LC50S-8 samples were completely out of range and therefore they were not plotted in the figure. However, due to their high results, these concretes were classified as Low performance and are not recommended for chloride environments. Samples 70LC30S-10 and 50LC50S-10 were also considered low-performance for aggressive environments even though they presented compressive strength over 50 MPa (Fig. 13). The results from theses samples were similar to those presented by Noushini & Castel with 75 % fly ash in the precursor [26]. The chloride bulk diffusion coefficients and Coulombs values of calcined clay-GGBFS alkali-activated concretes were higher than that of 100 % GGBFS specimens [36]. It can be attribute to the formation of more pore filling calcium silicate hydrate gels in alkali-activated concrete with 100 % GGBFS [43].

Regarding high-grade calcined clay samples, 70HC30S-10 was also considered low performance, this samples had similar results to Ferronickel slag (FNS) blended with GGBFS (Fig. 13). Nonetheless, the sample 50HG50S-10 was classified as having medium performance, similar to two reference concretes designated as OPC1 and OPC2. These reference samples were made with General-Purpose cement and exhibited average compressive strengths of 49 MPa and 64 MPa at 28 days, respectively. Geopolymer concretes in the medium-performance category could be used in some chloride environments with further investigations [1]. A recent study, considering fly ash or GGBFS based alkali-activated concreted, showed that the short-term bulk diffusion test results align well with the long-term performance of similar specimens exposed to a natural chloride environment [44]. Therefore, based on the performance-based criteria presented in Fig. 12, the results of the modified-RCPT 10V can also be an indicator of the long-term

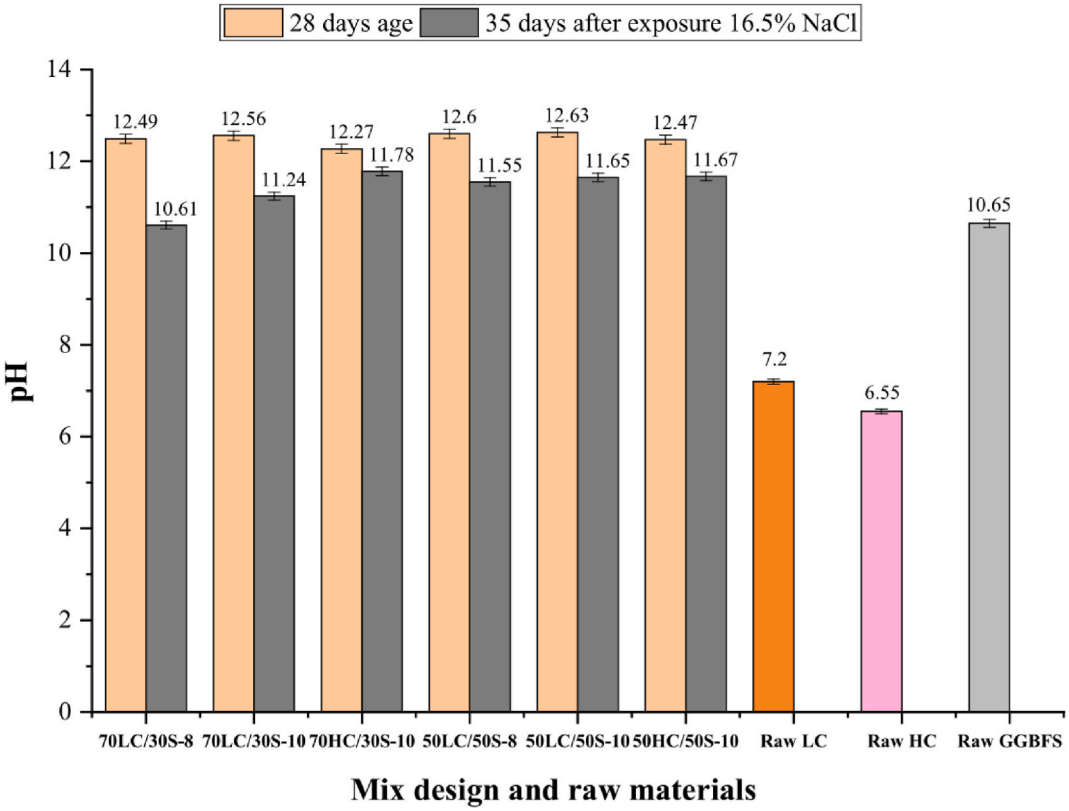

Fig. 14. pH measurement of leachate results at 28 days and 35 days after 165 g/L NaCl solution.

performance of alkali-activated calcined clay-GGBFS concretes exposed to natural chloride environments. However, more field data are required to establish a more accurate prediction of long-term performance based on modified-RCPT 10V for alkali-activated materials.

4.8. pH measurement of leachate

The pH values of leachate at 28 days and 35 days after exposure to a 165 g/L NaCl solution are presented in Fig. 14. Prior to the exposure, the samples showed varying pH levels ranging from 12.27 to 12.63. Notably, the sample consisting of high-grade calcined clay with an activation level of Na_2O equal to 10 % exhibited the lowest pH value (12.27). This finding is attributed to the inherent lower pH characteristics of HC-calcined clay compared to low grade calcined clay counterparts. The pH of all samples decreased after being exposed to a 165 g/L NaCl solution. The largest decreases in pH were observed in samples containing lower grade calcined clay, regardless of the proportion of precursor or the concentration of the alkaline activator used. Samples 70LC/30S-8, 70LC/30S-10, 50LC/50S-8, and 50LC/50S-10 registered pH values of approximately 10.61, 11.24, 11.55, and 11.65, respectively. In contrast, the samples 70HC/30S-10 and 50HC/50S-10 showed pH levels of 11.78 and 11.67, respectively. These results agree with the results of the porosity of the materials (Fig. 9(a)(b)) and are probably linked to the leaching of alkalis in the samples. For example, the 70LC30S-8 mix showed some efflorescence even before its exposure to the NaCl solution (Fig. 5), the same sample presented the highest cumulative porosity among the specimens tested.

Lloyd, Provis & Van Deventer examined the pore solutions of alkali-activated pastes incorporating fly ash and GGBFS [45]. The study identified a potential issue with the paste's capacity to retain alkalis, particularly when the material was exposed to water. The findings highlighted that alkali elements are highly mobile in the pore systems of these composite materials, and this could pose a risk to the durability of structures with embedded steel reinforcement. The research emphasized that the formulation of alkali-activated pastes had a critical role in limiting alkali movement. Specifically, the presence of calcium contributed to reducing alkali mobility by producing more C-A-S-H and enhancing the microstructure's density, thereby helping to maintain a high pH level.

4.9. XRD of alkali-activated pastes

The XRD analysis of alkali-activated samples containing calcined clay and GGBFS, cured for 28 days prior to exposure, is showed in Fig. 15. Depending on the specific precursor employed, the mixtures' crystalline profiles exhibited varied crystalline phases. For those blends utilizing low-grade calcined clay, distinctive peaks corresponding to elements like quartz, kaolinite, and certain zeolites were

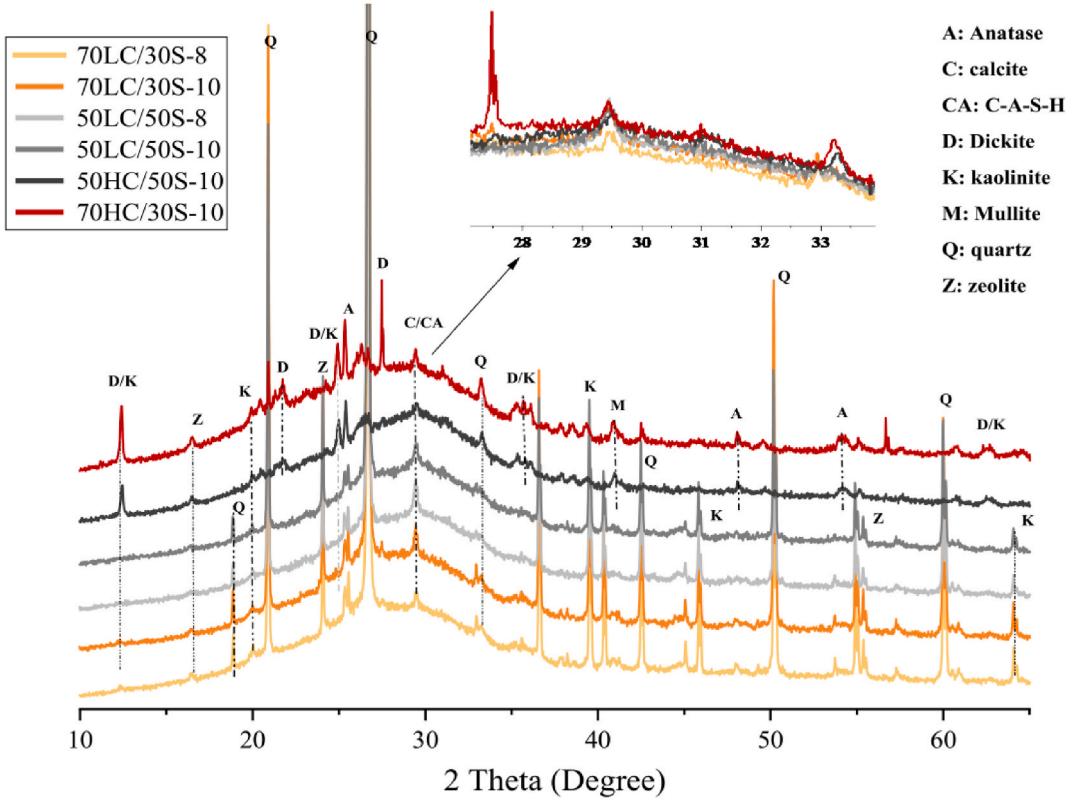

Fig. 15. XRD diffractograms of 28 days alkali-activated calcined clay/GGBFS.

observed. Similar, for those with high-grade calcined clay, the peaks aligned with the raw material (as shown in Fig. 1) such as dickite, mullite, kaolinite, quartz, and anatase. The XRD patterns of all samples displayed a broad peak at around 26° 2θ and 36° 2θ, indicating the presence of an amorphous phase associated with C-A-S-H gel formation. However, the mixture with a dominant presence of low-grade calcined clay and 8 % alkaline concentration (70LC30S-8) exhibited a diminished intensity in this peak, suggesting reduced dissolution and C-A-S-H formation.

Fig. 16 illustrates how chloride penetration impacts the mineral phases present in alkali-activated pastes after they've been exposed to a NaCl solution. Following exposure to the NaCl solution, no new phases emerged in the samples, except for the appearance of some crystalline NaCl (halite) with the low-grade calcined clay. Unlike what's typically seen in OPC samples, no formation of Friedel's salt was detected in any sample. A similar observation was made by Babaee & Castel [42]. However, their study involving fly ash and GGBFS, no new phases were detected either. A notable point is that, excluding the peak at 47.7° 2θ, halite peaks primarily appeared in samples containing a larger quantity of low-grade calcined clay. Specifically, sample 70LC30S-8 exhibited the most pronounced intensity for these peaks, which are identified at 31.7° 2θ and 56.5° 2θ. This finding aligns well with the data on porosity, apparent chloride diffusion coefficient, and pH reduction obtained specifically for this sample. Similarly, results for samples made with high-grade calcined clay, which did not show significant halite phases, are consistent with both porosity and apparent chloride coefficient measurements results. The lower porosity of the specimens with high-grade calcined clay could minimize the deposition of NaCl in the microstructure, leading to the absence of halite peaks.

N-A-S-H gels exhibit a more porous microstructure when compared to C-A-S-H gels. Even though N-A-S-H gels have a greater chloride binding capacity due to their larger surface area, their inferior pore structure adversely impacts their performance. Consequently, N-A-S-H gels are generally less resistant to chloride diffusion than C-A-S-H gels [9]. Yang et al. noted that halite was identified in the geopolymer sample composed solely of fly ash after it underwent NaCl tests [46]. They observed that apart from chloride ions physically adsorbed onto N-(A)-S-H gel, the unbound chloride could potentially react with the alkali metal cations present in the pore solution, eventually precipitating as halite during the drying or evaporation process.

5. Conclusions

This research investigated the effects of different precursors proportions, concentrations of alkali activator, and amorphous content in two types of calcined clays on chloride penetration resistance in binary calcined clay/GGBFS concretes. Several durability tests were conducted, including bulk chloride diffusion, modified-RCPT 10V, and NT Build 492 to evaluate how these concretes performed. Based on this analysis, several conclusions can be drawn about how these materials respond to chloride exposure.

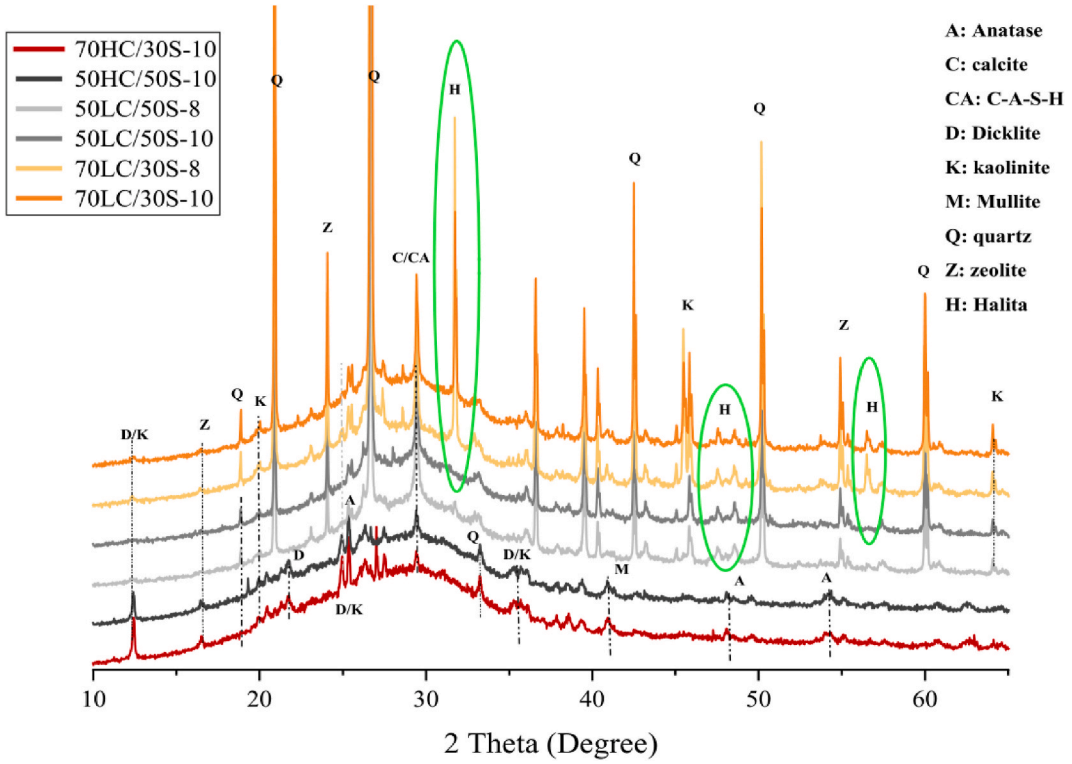

Fig. 16. XRD diffractograms of alkali-activated calcined clay/GGBFS pastes after 35 days exposure to NaCl solution.

1. The 28-day compressive strength of the calcined clay-GGBFS geopolymer concretes ranged from 31.5 to 63.5 MPa, making them suitable for structural applications in chloride environments. The highest compressive strength (63.5 MPa) was observed in the formulation with high-grade calcined clay and 10 % Na_2O, while the lowest (31.5 MPa) was seen in the mix with low-grade calcined clay and 8 % Na_2O.
2. The transport properties improved with higher Na_2O concentrations, as water absorption and permeable voids decreased, especially in samples with high-grade calcined clay due to an increased dissolution of the aluminosilicate phases, which resulted in a denser microstructure.
3. Bulk and surface resistivity tests, along with modified-RCPT, were influenced by presence of free ions in the pore solution, leading to increased the charge transfer. The D_{nssm} values ranged from 33.74 to 177.98 ($\times 10^{-12}$ m^2/s), with the 50HC50S-10 sample (high-grade calcined clay) achieving the lowest value.
4. Low-grade calcined clay samples with 8 % Na_2O showed a poor chloride penetration resistance ($D_a > 300 \times 10^{-12}$ m^2/s), but increasing Na_2O to 10 % improved their performance. High-grade calcined clay further reduced D_a values to around 27.0 and 42.29 ($\times 10^{-12}$ m^2/s), significantly enhancing the chloride penetration resistance.
5. RCPT results correlated well with the chloride diffusion coefficients. Most samples were low-performing in chloride environments, except for the 50HG50S-10 mix, which demonstrated comparably to OPC reference concretes with compressive strength of 50 MPa and 60 MPa.
6. No new phases were detected after exposure to NaCl, except for halite formation in low-grade calcined clay samples due to unbound chloride ions. Friedel's salt was not observed in any sample, unlike in OPC mixes.

The findings indicate that alkali-activated concretes, particularly those incorporating slag and calcined clays, demonstrate promising potential for coastal or marine applications due to their enhanced to chloride resistance and mechanical properties. By optimising the mix composition, calcined clay-GGBFS alkali-activated materials can achieve an average compressive strength above 50 MPa, meeting the requirements for various structural applications for buildings and infrastructures. The dense microstructure formed by C-A-S-H and N-A-S-H gels, as confirmed in the XRD analysis, significantly reduces chloride ingress, a critical factor in ensuring durability in chloride-rich environments. In addition, the usage of high-reactivity calcined clay could further improve chloride resistance of calcined clay – GGBFS alkali-activated concretes. Nevertheless, some limitations should be acknowledged, including the variability in raw material reactivity and the complexities associated with optimising the alkali activator concentration for large-scale production.

Future research should focus on evaluating the long-term performance of these concretes under real-world marine conditions, assessing the environmental impact of alkali activators, and developing standardised guidelines for their application in marine

infrastructure. Moreover, further investigation of different calcined clays to enhance both performance and cost-efficiency would be valuable.

CRediT authorship contribution statement

Samuel De Carvalho Gomes: Writing – original draft, Visualization, Methodology, Investigation, Formal analysis, Data curation, Conceptualization. **Yu Pang:** Writing – review & editing, Writing – original draft, Visualization, Investigation, Formal analysis, Data curation. **Quang Dieu Nguyen:** Writing – review & editing, Supervision, Project administration, Methodology, Investigation, Formal analysis, Conceptualization. **Wengui Li:** Writing – review & editing, Supervision, Investigation. **Kirk Vessalas:** Writing – review & editing, Supervision, Investigation. **Arnaud Castel:** Writing – review & editing, Supervision, Project administration, Investigation, Funding acquisition, Conceptualization.

Declaration of competing interest

The authors declare that they have no known competing financial interests or personal relationships that could have appeared to influence the work reported in this paper.

Acknowledgements

The authors would like to thank the School of Civil and Environmental Engineering, University of Technology Sydney (UTS) - Tech Lab, Sydney, NSW for providing technical support.

Data availability

Data will be made available on request.

References

[1] Q.D. Nguyen, S. De Carvalho Gomes, M.F. Alnahhal, W. Li, T. Kim, A. Castel, Testing Geopolymer Concrete Performance in Chloride Environment, vol. 44, RILEM Bookseries, 2023, pp. 1197–1203.
[2] G. Yang, J. Zhao, Y. Wang, Durability properties of sustainable alkali-activated cementitious materials as marine engineering material: a review, Mater. Today Sustain. 17 (2022) 100099.
[3] X. Zhang, K. Long, W. Liu, L. Li, W.-J. Long, Carbonation and chloride ions' penetration of alkali-activated materials: a review, Molecules 25 (2020) 5074.
[4] X. Ke, S.A. Bernal, J.L. Provis, Uptake of chloride and carbonate by Mg-Al and Ca-Al layered double hydroxides in simulated pore solutions of alkali-activated slag cement, Cement Concr. Res. 100 (2017) 1–13.
[5] B. Zhang, H. Zhu, P. Feng, P. Zhang, A review on shrinkage-reducing methods and mechanisms of alkali-activated/geopolymer systems: effects of chemical additives, J. Build. Eng. 49 (2022) 104056.
[6] J. Zhang, Y. Ma, J. Hu, H. Wang, Z. Zhang, Review on chloride transport in alkali-activated materials: role of precursors, activators and admixtures, Constr. Build. Mater. 328 (2022) 127081.
[7] Y. Liu, W. Zhu, E.-H. Yang, Alkali-activated ground granulated blast-furnace slag incorporating incinerator fly ash as a potential binder, Constr. Build. Mater. 112 (2016) 1005–1012.
[8] A. Runci, M. Serdar, Chloride-induced corrosion of steel in alkali-activated mortars based on different precursors, Materials 13 (2020) 5244.
[9] W. Tahri, X. Hu, C. Shi, Z. Zhang, Review on corrosion of steel reinforcement in alkali-activated concretes in chloride-containing environments, Constr. Build. Mater. 293 (2021) 123484.
[10] B.A. Salami, M. Ibrahim, H.A. Algaifi, W. Alimi, A.O. Ewebajo, A review on the durability performance of alkali-activated binders subjected to chloride-bearing environment, Constr. Build. Mater. 317 (2022) 125947.
[11] A. Heath, K. Paine, M. McManus, Minimising the global warming potential of clay based geopolymers, J. Clean. Prod. 78 (2014) 75–83.
[12] I. Garcia-Lodeiro, A. Palomo, A. Fernández-Jiménez, D.E. Macphee, Compatibility studies between N-A-S-H and C-A-S-H gels. Study in the ternary diagram Na 2O–CaO–Al 2O 3–SiO 2–H 2O, Cement Concr. Res. 41 (2011) 923–931.
[13] I. Ismail, S.A. Bernal, J.L. Provis, R. San Nicolas, D.G. Brice, A.R. Kilcullen, S. Hamdan, J.S.J. van Deventer, Influence of fly ash on the water and chloride permeability of alkali-activated slag mortars and concretes, Constr. Build. Mater. 48 (2013) 1187–1201.
[14] N.K. Lee, H.K. Lee, Influence of the slag content on the chloride and sulfuric acid resistances of alkali-activated fly ash/slag paste, Cement Concr. Compos. 72 (2016) 168–179.
[15] N.R. Rakhimova, V.P. Morozov, A.A. Eskin, Y.S. Lutskin, O.S. Shynkevych, Blended alkali-activated cements based on blast-furnace slag and calcined clays: statistical modeling and effect of amount and chemistry of reactive phase, J. Mater. Civ. Eng. (2022) 34.
[16] G. Huang, Y. lv, S. Ren, Y. Liao, X.-Y. Wang, R. Guo, R.-S. Lin, Production of low-CO2 ternary binder using red sandstone, cement, and granulated blast furnace slag: a comprehensive performance analysis, Constr. Build. Mater. 431 (2024) 136576.
[17] S.D.C. Gomes, Q.D. Nguyen, W. Li, A. Castel, Carbonation resistance of calcined clay-ground granulated blast furnace slag alkali-activated mortar, Constr. Build. Mater. 393 (2023) 131811.
[18] S.D.C. Gomes, Q.D. Nguyen, W. Li, A. Castel, Effects of mix composition on the mechanical, physical and durability properties of alkali-activated calcined clay/slag concrete cured under ambient condition, Constr. Build. Mater. 453 (2024) 139064.
[19] Q.D. Nguyen, S. Afroz, A. Castel, Influence of calcined clay reactivity on the mechanical properties and chloride diffusion resistance of limestone calcined clay cement (LC3) concrete, J. Mar. Sci. Eng. 8 (2020) 301.
[20] R. Bajpai, K. Choudhary, A. Srivastava, K.S. Sangwan, M. Singh, Environmental impact assessment of fly ash and silica fume based geopolymer concrete, J. Clean. Prod. 254 (2020) 120147.
[21] J.L. Provis, Alkali-activated materials, Cement Concr. Res. 114 (2018) 40–48.
[22] A. C39/C39M-18, Standard Test Method for Compressive Strength of Cylindrical Concrete Specimens, ASTM International, West Conshohocken, PA, 2018.
[23] ASTM C642-13, Standard Test Method for Density, Absorption, and Voids in Hardened Concrete, ASTM International, West Conshohocken, PA, 2013.
[24] AASHTO T 358-19, Standard Method of Test for Surface Resistivity Indication of Concrete's Ability to Resist Chloride Ion Penetration, 2019.
[25] A. Noushini, A. Castel, The effect of heat-curing on transport properties of low-calcium fly ash-based geopolymer concrete, Constr. Build. Mater. 112 (2016) 464–477.

[26] A. Noushini, A. Castel, Performance-based criteria to assess the suitability of geopolymer concrete in marine environments using modified ASTM C1202 and ASTM C1556 methods, Mater. Struct. 51 (2018) 1–16.
[27] A. Noushini, Q.D. Nguyen, A. Castel, Assessing alkali-activated concrete performance in chloride environments using NT Build 492, Mater. Struct. (2021) 54.
[28] NT Build 492, (1999) Concrete, mortar and cement-based repair materials: chloride migration coefficient from non-steady-state migration experiments, Nordtest, Espoo, Finland (1999-11).
[29] ASTM C1556 Test Method for Determining the Apparent Chloride Diffusion Coefficient of Cementitious Mixtures by Bulk Diffusion.
[30] ASTM C1152/C1152M Standard Test Method for Acid-Soluble Chloride in Mortar and Concrete, ASTM International, West Conshohocken, PA.
[31] R. Snellings, J. Chwast, Ö. Cizer, N. De Belie, Y. Dhandapani, P. Durdzinski, J. Elsen, J. Haufe, D. Hooton, C. Patapy, M. Santhanam, K. Scrivener, D. Snoeck, L. Steger, S. Tongbo, A. Vollpracht, F. Winnefeld, B. Lothenbach, RILEM TC-238 SCM recommendation on hydration stoppage by solvent exchange for the study of hydrate assemblages, Mater. Struct. 51 (2018) 1–4.
[32] M.S.H. Khan, A. Castel, Effect of MgO and Na2SiO3 on the carbonation resistance of alkali activated slag concrete, Mag. Concr. Res. 70 (2018) 685.
[33] M.S.H. Khan, Q.D. Nguyen, A. Castel, Performance of limestone calcined clay blended cement-based concrete against carbonation, Adv. Cement Res. 32 (2020) 481–491.
[34] Q.D. Nguyen, M.S.H. Khan, A. Castel, Chloride diffusion in limestone flash calcined clay cement concrete, ACI Mater. J. 117 (2020).
[35] A. Noushini, Q.D. Nguyen, A. Castel, Assessing alkali-activated concrete performance in chloride environments using NT Build 492, Mater. Struct. 54 (2021) 57.
[36] A. Noushini, A. Castel, Performance-based criteria to assess the suitability of geopolymer concrete in marine environments using modified ASTM C1202 and ASTM C1556 methods, Mater. Struct. 51 (2018) 146.
[37] S. Mindess, F. Young, D. Darwin, Concrete 2nd Editio, Technical Documents, 2003, p. 585.
[38] H. Alanazi, J. Hu, Y.-R. Kim, Effect of slag, silica fume, and metakaolin on properties and performance of alkali-activated fly ash cured at ambient temperature, Constr. Build. Mater. 197 (2019) 747–756.
[39] Q.D. Nguyen, M.S.H. Khan, A. Castel, T. Kim, Durability and microstructure properties of low-carbon concrete incorporating Ferronickel slag sand and fly ash, J. Mater. Civ. Eng. (2019) 31.
[40] S.A. Bernal, R. Mejía de Gutiérrez, J.L. Provis, Engineering and durability properties of concretes based on alkali-activated granulated blast furnace slag/metakaolin blends, Constr. Build. Mater. 33 (2012) 99–108.
[41] AS 3600, Concrete Structures, Standards Australia, Sydney, Australia, 2018.
[42] M. Babaee, A. Castel, Chloride diffusivity, chloride threshold, and corrosion initiation in reinforced alkali-activated mortars: role of calcium, alkali, and silicate content, Cement Concr. Res. 111 (2018) 56–71.
[43] J.L. Provis, R.J. Myers, C.E. White, V. Rose, J.S.J. van Deventer, X-ray microtomography shows pore structure and tortuosity in alkali-activated binders, Cement Concr. Res. 42 (2012) 855–864.
[44] D. Law, Y. Patrisia, C. Gunasekara, A. Castel, Q.D. Nguyen, A. Wardhono, Durability assessment of alkali-activated concrete exposed to a marine environment, J. Mater. Civ. Eng. 35 (2023) 04023275.
[45] R.R. Lloyd, J.L. Provis, J.S.J. van Deventer, Pore solution composition and alkali diffusion in inorganic polymer cement, Cement Concr. Res. 40 (2010) 1386–1392.
[46] T. Yang, X. Yao, Z. Zhang, Quantification of chloride diffusion in fly ash–slag-based geopolymers by X-ray fluorescence (XRF), Constr. Build. Mater. 69 (2014) 109–115.